nature geoscience

ARTICLES

PUBLISHED ONLINE: 16 OCTOBER 2017 | DOI: 10.1038/NGEO3046

Substantial export of suspended sediment to the global oceans from glacial erosion in Greenland

I. Overeem[1]*, B. D. Hudson[1,2], J. P. M. Syvitski[1], A. B. Mikkelsen[3], B. Hasholt[3], M. R. van den Broeke[4], B. P. Y. Noël[4] and M. Morlighem[5]

Limited measurements along Greenland's remote coastline hamper quantification of the sediment and associated nutrients draining the Greenland ice sheet, despite the potential influence of river-transported suspended sediment on phytoplankton blooms and carbon sequestration. Here we calibrate satellite imagery to estimate suspended sediment concentration for 160 proglacial rivers across Greenland. Combining these suspended sediment reconstructions with numerical calculations of meltwater runoff, we quantify the amount and spatial pattern of sediment export from the ice sheet. We find that, although runoff from Greenland represents only 1.1% of the Earth's freshwater flux, the Greenland ice sheet produces approximately 8% of the modern fluvial export of suspended sediment to the global ocean. Sediment loads are highly variable between rivers, consistent with observed differences in ice dynamics and thus with control by glacial erosion. Rivers that originate from deeply incised, fast-moving glacial tongues form distinct sediment-export hotspots: just 15% of Greenland's rivers transport 80% of the total sediment load of the ice sheet. We conclude that future acceleration of melt and ice sheet flow may increase sediment delivery from Greenland to its fjords and the nearby ocean.

Rivers are prime conveyors of material on the Earth's surface[1,2] and move 56% of sediment entering the ocean[3]. Fluvial delivery affects coastal zone dynamics, marine ecosystems, and ocean biogeochemistry. For example, increased suspended sediment delivery impacts ecosystem dynamics, either reducing light availability and thus limiting primary productivity, or by carrying bioavailable micronutrients, which enhance phytoplankton blooms[4–7]. Whereas the conveyance of sediment to the ocean is characterized for most of the world's rivers, reconstructions for Greenland and the Greenland ice sheet (GrIS) are lacking, despite indication of disproportional amounts of sediment originating from other glaciated regions[8–10].

The need for a sound estimate of the sediment flux coming out of Greenland is even more pressing since the GrIS is in decay, and glacial processes that control bedrock erosion may be accelerating. Reconciled estimates from satellite methodologies and modelling find that over 2005–2010 the GrIS lost $\sim$263 Gt yr^{-1} (ref. 11), whereas over the most recent few years (2009–2012) mass loss amounted to $-$380 Gt yr^{-1} (refs 12,13). Outlet glaciers accelerated rapidly over the early 2000s and continued this trend over the past decade[14,15], but have stabilized since 2005[12,16].

To constrain the sediment contribution from Greenland to the North Atlantic Ocean and Arctic Ocean, in view of possible glacial erosion regime accelerations, we develop a satellite data analysis technique to quantify proglacial river sediment concentrations around the entire GrIS margin.

We present remote sensing techniques that vastly expand our capability to measure suspended sediment concentration (SSC) in remote regions[17]. The techniques allow us to compile a data set for 160 Greenlandic rivers, and offer detailed maps of regional sediment delivery to the fjords. Compared to previous studies[5,18], we offer an order of magnitude more data to investigate the primary controls on sediment flux magnitude at individual outlets.

Measurements of river sediment concentration

A riverine suspended sediment concentration retrieval algorithm for Landsat7 Enhanced Thematic Mapper and Earth Observation-1 Advanced Land Imager (ALI) imagery is developed. *In situ* measurements of sediment concentration from the only comprehensively monitored river in Greenland, the Watson River near Kangerlussuaq, (Supplementary Fig. 1), significantly correlate with remotely sensed reflectance of visible and near-infrared light as measured with Landsat7 and ALI ($r^2 = 0.90$, $p < 0.01$, $n = 49$, details in Methods, Supplementary Fig. 2 and Supplementary Table 1). A robust retrieval algorithm for fjord SSC and the Moderate Resolution Imaging Spectroradiometer (MODIS) reflectance in the visible light spectrum over vastly different fjords in West Greenland provides support for extrapolation beyond a single river system[17].

Using the online, massively parallel processing capability of Google Earth Engine, we apply our SSC retrieval algorithm to all cloud-free Landsat7 images of Greenland (over 1999–2013). Since temporal resolution is limited by the 16-day repeat interval of Landsat imaging, and cloud cover can further reduce data availability, we reconstruct a 'long-term' sediment concentration for each proglacial outlet. Sediment concentration is analysed over the active river discharge summer season (day 160–240) for all 14 years. We analyse 160 suitable rivers throughout Greenland. This compilation of imagery guarantees we include a number of large discharge events for each river, and thus honour the highly nonlinear nature of sediment transport by including some of the potentially most impactful transport events in our calculations. A total of 5,760

[1]Community Surface Dynamics Modeling System, INSTAAR, University of Colorado, Boulder, Colorado 80303, USA. [2]Polar Science Center, Applied Physics Laboratory, University of Washington, Seattle, Washington 98105, USA. [3]Department of Geoscience and Natural Resource Management, University of Copenhagen, 1350 Copenhagen, Denmark. [4]IMAU, Utrecht University, 3584 CC Utrecht, the Netherlands. [5]Department of Earth System Science, University of California, Irvine, California 92697, USA. *e-mail: irina.overeem@colorado.edu

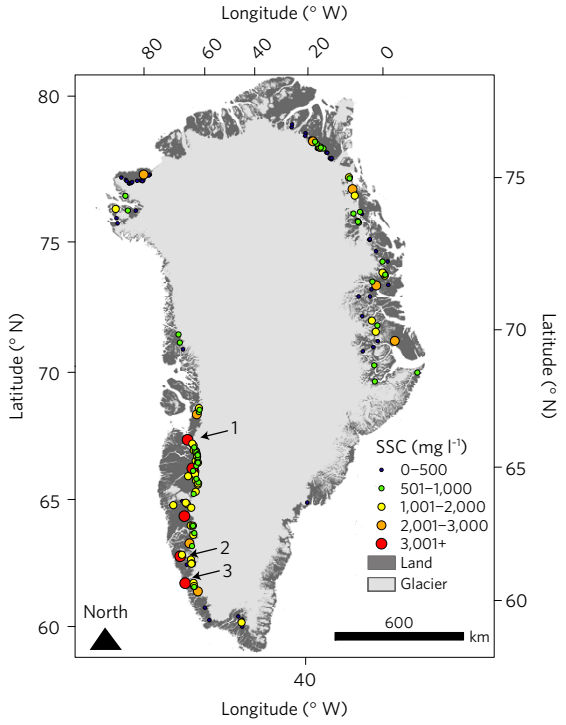

Figure 1 | Map of long-term proglacial riverine suspended sediment concentration (SSC) for 160 selected rivers along the Greenland ice sheet margin. Only land terminating, non-lake outlets were imaged, thus certain regions of the GrIS are not considered (for example, Southeast Greenland). Distinct hotspots of sediment export are located in West Greenland. 1, Akuliarutsjip; 2, Sermeq; 3, Sioqqap Sermia.

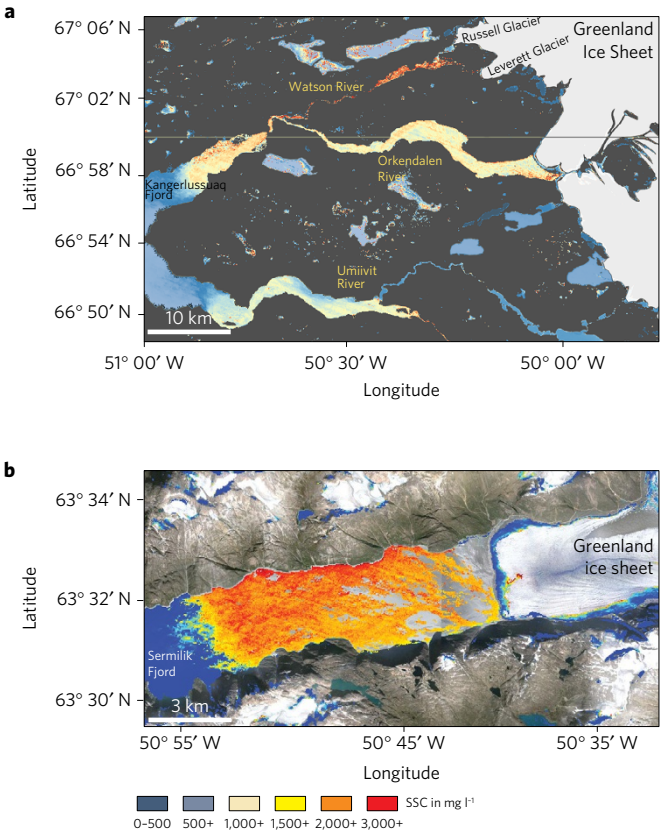

Figure 2 | Maps of the mean suspended sediment concentration (SSC) derived from the Landsat7 image analysis over 1999–2014. a, Map of the river braidplains of the Watson and Örkendalen rivers, West Greenland. Nearby glacial outlets, that is, the Russell and Leverett glacial outlets, experience a similar surface mass balance but show distinctly different long-term sediment concentrations. **b**, Map of the river braidplain of Sermeq Glacier draining into Sermilik Fjord just south of Nuuk, West Greenland.

Landsat7 images are included (each river outlet over 14 years is constrained by between 11 and 109 images).

The selected river outlets include seven out of ten of the largest GrIS meltwater outlets (as inferred from runoff reconstructions based on RACMO2.3). The other three major outlets feature tidewater glaciers calving directly into fjords and cannot be directly measured; these are instead incorporated through subsequent process-based extrapolation. By design, the analysis omits a few outlets with large proglacial lakes, especially in South Greenland, because we assume incoming sediment is efficiently trapped within lakes and does not contribute to sediment flux to the marine environment.

We hypothesize that glacio-hydrology, ice dynamics and lithology are the main controls on sediment concentration in the proglacial rivers of Greenland. We use state-of-the-art surface elevation, ice thickness, ice surface velocity, and geologic data sets to explain the observed spatial patterns in suspended sediment concentration. Meltwater runoff is calculated using a regional-atmospheric model coupled to a surface mass balance ice model (RACMO2.3) (refs 19,20) allowing for a total summer meltwater discharge per glacio-hydrological catchment to be calculated. Annual sediment load per river outlet is then calculated as the product of discharge, Q_{mc}, and sediment concentration, SSC. High-quality ice thickness data coverage is limited to certain regions of the GrIS, thus the regression analysis comprises a subset of just 53 rivers (details on data set processing in Methods).

Hotspots of sediment export

A relatively small number of GrIS glacio-hydrological catchments feature high sediment concentration (Fig. 1). Most (67%) termini discharge melt water with median SSC values $<1{,}000\,mg\,l^{-1}$, while 8% of the proglacial rivers show SSC values $>2{,}000\,mg\,l^{-1}$ (Supplementary Table 2). Often GrIS-fed rivers convey relatively low SSC water, the median SSC of examined Greenlandic rivers was found to be $992\,mg\,l^{-1}$. Despite relatively low median SSC values found, some outlets are distinct sediment-export hotspots.

Even at the local scale, long-term river sediment concentration is remarkably variable. Figure 2a shows mean sediment concentration maps for the Watson River and Örkendalen River as compiled from all available Landsat7 imagery. Long-term sediment concentrations are distinctly higher for some tributaries, compared to nearby outlets. Figure 2a shows that the Leverett Glacier outlet contributes on average five times more suspended sediment load to the Watson River than does the Russell Glacier outlet. Similarly, in the Örkendalen River, two proglacial outlets in close proximity that experience similar climate and melt regimes show consistently different suspended sediment concentrations over 1999–2012. As an example of a high-sediment outlet, the Sermeq outlet in Sermilik Fjord, south of Nuuk, is depicted in Fig. 2b, (outlet 16 in Supplementary Table 2). This outlet exports 25% of the total suspended load measured around the entire GrIS margin.

Control by ice dynamics

To explain the variability in long-term sediment-export observations, we conduct a stepwise regression analysis using a range of parameters averaged for each contributing glacio-hydrological catchment over the zone of active surface melt, including ice thickness[21], surface elevation[22], RACMO2.3-modelled runoff[19,20], that defines the total meltwater discharge, ice velocity[23] and

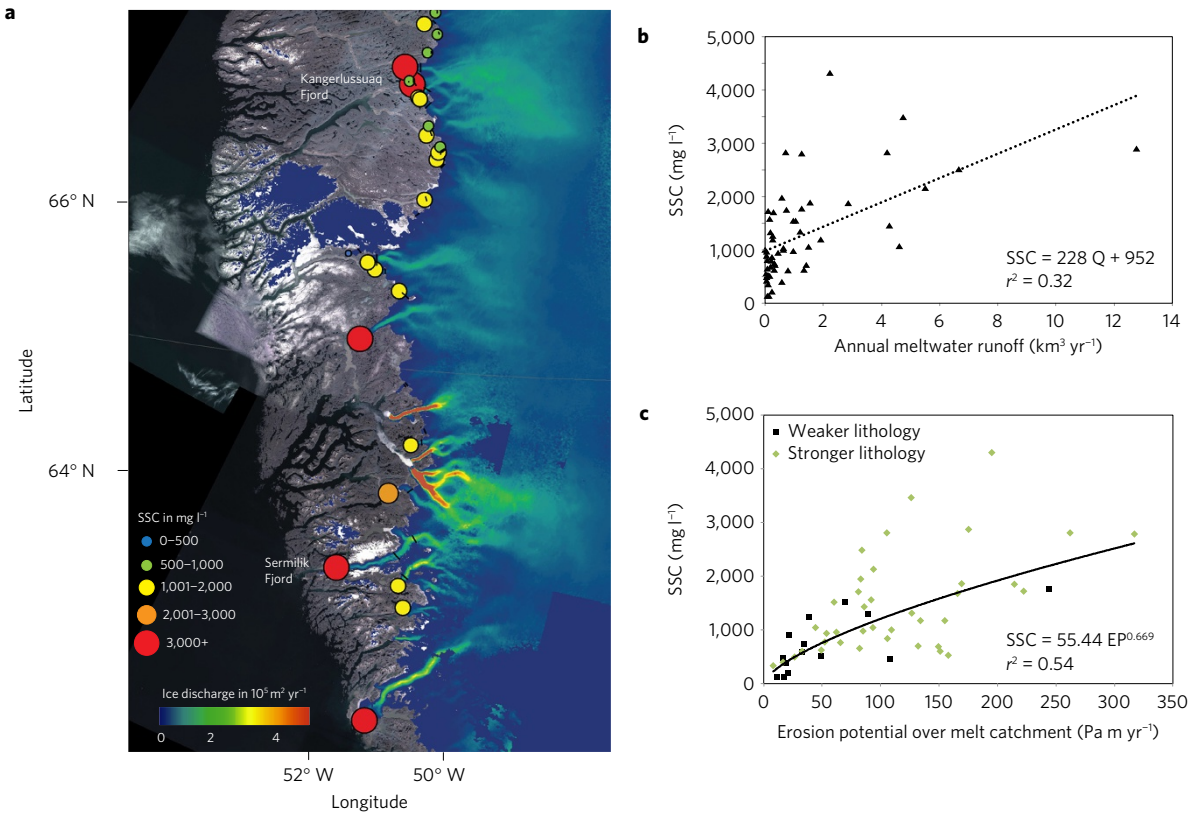

Figure 3 | Glacial dynamics control variability in suspended sediment delivery. a, Map of long-term river sediment concentration showing upstream mean ice discharge for Southwest Greenland. High ice discharge in the upstream melt catchment induces high suspended sediment concentrations. **b**, Meltwater runoff for specific river catchments shows weak positive correlation with its river's long-term SSC. **c**, Relationship between glacial erosion potential and long-term SSC. Black squares are outlets in regions with weaker rock strength, grey diamonds represent river outlets in regions with more resistant rock types. Lithology in the region of the river mouth has no conclusive control on suspended sediment concentration.

geology[24]. Analysis reveals that although meltwater flux explains some of the variation in SSC (Fig. 3b), suspended sediment concentration is more pronouncedly controlled by ice dynamics (see Methods, Fig. 3).

We postulate a simplified model for glacial erosion potential, EP, assuming erosion is at first order related to the basal sliding rate, u_s, and the gravitational driving stress of the ice mass, but without taking into account the detailed controls of seasonal variation in water pressure at the bed:

$$\mathrm{EP} = u_s \tau = 0.8 u_{surf} \rho_{ice} g\ h_{ice} S \quad (1)$$

where u_s is the basal sliding ice velocity (m yr^{-1}), τ is the shear stress (Pa), h_{ice} is the ice thickness (m) and S is the local surface slope (-). We assume $u_s = a\ u_{surf}$ (with $a = 0.8$ (-)) to arrive at bed sliding ice velocity, u_s, from observed surface velocity, u_{surf}. Furthermore, the density of ice, ρ_{ice}, is 900 kg m^{-3}, and the acceleration of gravity, g, is 9.8 m s^{-1}. We calculate the mean erosion potential (EP_{mean}) for each hydrologic catchment to derive a relationship between erosion potential and the suspended sediment produced by each catchment:

$$\mathrm{SSC} = 55.4 \mathrm{EP}_{mean}^{0.669} \quad (2)$$

where SSC is in mg l^{-1}, EP in Pa m yr^{-1}. Equation (2) explained 54% of the data variance ($r^2 = 0.54$, $p < 0.0001$, $n = 53$, Fig. 3c).

River sediment concentrations do not appear to be strongly affected by lithology (Fig. 3c); correlation between mapped lithology at the locality of the proglacial river, its assigned rock strength, and SSC is inconclusive. Subglacial lithology is not accurately known, neither is the amount of sediment or till accumulated at the base of the ice sheet, thus either of those factors may obscure a direct relation between outlet lithology and SSC.

Previous reconstructions of solutes originating from Greenland are extrapolations of single catchment characteristic concentrations to all proglacial rivers and multiply by the modelled total GrIS water runoff. Using the newly reconstructed SSC, total sediment load for the entire GrIS would amount to 1.28 ± 0.51 Gt yr^{-1}, according to this meltwater-based extrapolation method (see Methods).

However, since we find that SSC is dominantly controlled by glacial dynamics, we here use an alternate, more process-based, approach and apply the newly derived proglacial river sediment load relationship to extrapolate to glacio-hydrological catchments that could not be directly assessed by the satellite measurement technique. If we use equation (2) to determine riverine suspended sediment concentration for all contributing glacio-hydrological catchments around the GrIS and multiply these by their mean annual modelled meltwater discharge (details in Methods), we find that the GrIS and associated small ice caps export 0.892 ± 0.374 Gt of suspended sediment annually.

A significant portion of the GrIS flows to tidewater glacier outlets. There, glacier calving fronts discharge icebergs, which obscure sediment-rich water, and sediment is transported internally and at the base of icebergs. Upwelling meltwater plumes occur at the base of calving ice fronts at water depths of hundreds of metres and are not detectable from space. However, our analysis shows that SSC is controlled dominantly by glacier dynamics, and thus suspended sediment flux at tidewater outlets has been included in the above sediment budget on the assumption that equation (2) holds for meltwater funnelled through tidewater glaciers.

Table 1 | Melt water and sediment flux from Greenland.

Greenland regions	Water discharge		SSC based on meltwater flux method	SSC based on glacier erosion method
	Q_w (km^3 yr^{-1})*	Q_w (%)	Q_s (Gt yr^{-1})	Q_s (Gt yr^{-1})
Baffin Bay	126	28%	0.363	0.371
Denmark Strait	60	13%	0.173	0.150
Davis Strait	173	39%	0.497	0.243
Greenland Sea	48	11%	0.138	0.084
Scoresby Sound	10	2%	0.030	0.021
Arctic Ocean	28	6%	0.082	0.023
Total river meltwater flux	446	44%	1.28	0.892
Ice calving flux†	576	56%	0.014	0.014
Total Transport	1,022	100%	1.294	0.906
Basal ice calving flux‡	5.7	1%	1.92	n/a

Continents	Water discharge		Suspended sediment	
	Q_w (km^3 yr^{-1})	Q_w (%)	Q_s (Gt yr^{-1})	Q_s (%)
Africa§	3,797	9.6	1.1	8
Asia§	9,806	24.8	4.8	34
Australasia§	608	1.5	0.28	2
Europe§	2,680	6.8	0.4	3
Indonesia§	4,251	10.8	2.4	17
North America§	5,819	14.7	1.5	11
Oceans§	20	0.1	0.004	0
South America§	11,529	29.2	2.4	17
GLOBAL§	38,510	97.4	12.884	91
Greenland melt	446	1.1	0.91–1.28	7–9
Greenland calving†	576	1.5	0.014	0
REVISED GLOBAL	39,532	100.0	14.18	100

*Total runoff for all delineated catchments draining from Greenland (RACMO2.3, 1999–2013), see Methods. †Average calving ice discharge from ice flux at the grounding line (2000–2012)[12]. ‡See Methods for englacial and basal sediment flux reconstruction. §Data from ref. 2.

To further complete the sediment budget, we used GrIS calving discharge reconstructions[12] to estimate contributions from englacial and basal sediment, which combined comprises ice-rafted debris. Englacial sediment, debris and dust held throughout the ice column, will be released over the entire period of melt of calved icebergs. This component of ice-rafted sediment will have higher travel distances. In terms of sediment budget, englacial sediments may be classified to be most similar to suspended sediment delivered by proglacial river discharge. We find that englacial sediment delivers only ∼14 Mt yr^{-1} to fjords and the North Atlantic Ocean. However, basal ice has high debris content, an unsorted mix of fine sediments, sand, pebbles, cobbles and boulders, due to shear of glacial ice on the bed and debris entrainment. Sparse field observations provide constraints on estimates for average basal sediment layer thickness (∼3 m) and concentration by volume (∼20%). Basal sediment and debris-rich ice delivers an estimated 2.88 Gt yr^{-1} to the ocean (see Methods).

Greenland's suspended sediment flux to the ocean

Modern riverine suspended sediment load to the coastal ocean has previously been quantified as 12.8 ± 0.5 Gt yr^{-1} (ref. 2). Thus, Greenland's rivers contribute 7–9% on top of the global modern fluvial load. This sediment flux from Greenland is disproportionally large, considering that Greenland melt water represents only 1.1% of the Earth's freshwater flux.

A large supply of fine-grained sediment with associated labile nutrients, including iron, from Greenland to the high-latitude sectors of the North Atlantic possibly has implications for regional phytoplankton blooms[25]. Whether Greenlandic fjords and coastal zones are a carbon sink, due to abundant blooms throughout the spring and summer[26], is a matter of ongoing debate. Our data set indicates that the combined river sediment load from the western margin of the GrIS is more than double (0.52 Gt yr^{-1}) that of the eastern margin (0.26 Gt yr^{-1}) and much exceeds the contribution of the northern margin (0.02 Gt yr^{-1}) (Table 1). Although changes in sea ice coverage, sea surface temperature, salinity and circulation all impact primary productivity, our analysis quantifies suspended sediment contributions for individual river sources, warranting more in-depth observations and analysis that would relate sediment and micronutrient supply and then allow better assessment of its role in the observed productivity.

Our compilation relies on a reflectance–SSC retrieval algorithm calibrated for proglacial river outlets. Additional observations of suspended sediment concentrations for fast-flowing tidewater glacier systems will continue to improve the overall sediment budget estimate. However, another pressing need may be to quantify the retention and storage of the suspended sediment within the fjords. Fjords are known to be pronounced sediment and carbon traps[10,27], and generally are classified as the most efficient filters of all estuary types[28]. Greenlandic fjords are long; the average pathway to the open ocean for the 160 outlets monitored is 89 ± 66 km. For example, the river draining Akuliarutsjip Glacier (Fig. 1) ranks second in sediment flux, but the regional fjord system is a labyrinth, with the shortest, tortuous pathway to the open ocean being ∼105 km.

Our analysis predicts tidewater margins to be high sediment producers on account of high glacial velocity, but the delivery of sediment-laden meltwater plumes upwelling from deep down the calving front do restrict the travel distance of the suspended sediment[29,30]. We postulate that hotspots for flux delivery to the ocean system probably need to be short fjords, much like the Sermilik Fjord (23 km) and Sioqqap Sermia (0 km) (Fig. 1) draining directly in Baffin Bay and Davis Strait.

Fjord geometry is relatively stable, and thus the spatial distribution of sediment sources and filtering capability with respect to

the marine domain is expected to have been relatively unchanged over the past few decades. However, ice dynamics have recently accelerated by ~16% (2000–2012)[14], with a slightly dampened but positive effect on sediment concentrations along affected outlets (~12%, as predicted from equation (2)). In addition, meltwater runoff flux is modelled to have changed by ~40% in comparison to the period 1961–1990[16]. We infer that present-day sediment flux to the ocean from Greenland is approximately 56% higher than during the baseline period of 1961–1990.

Provided sediment production is dominantly controlled by ice flow dynamics, any future acceleration of ice flow rates amplifies Greenland's sediment supply to the nearby ocean. Yet, a sustained negative surface mass balance and a large meltwater flux are required to transport sediments when produced by accelerated erosion.

Methods

Methods, including statements of data availability and any associated accession codes and references, are available in the online version of this paper.

Received 27 March 2017; accepted 14 September 2017; published online 16 October 2017

References

1. Walling, D. E. Human impact on land–ocean sediment transfer by the world's rivers. *Geomorphology* **79,** 192–216 (2006).
2. Syvitski, J. P. M. & Kettner, A. J. Sediment flux and the Anthropocene. *Phil. Trans. R. Soc. A.* **369,** 957–975 (2011).
3. Syvitski, J. P. M., Kettner, A. J., Overeem, I., Brakenridge, R. & Cohen, S. *Latitudinal Controls on Stratigraphic Models and Sedimentary Concepts* (SEPM Special Publication, in the press, 2017).
4. Arrigo, K. R. Carbon cycle: marine manipulations. *Nature* **450,** 491–492 (2007).
5. Bhatia, M. P. *et al*. Greenland meltwater as a significant and potentially bioavailable source of iron to the ocean. *Nat. Geosci.* **6,** 274–278 (2013).
6. Sanders, R. *et al*. The biological carbon pump in the North Atlantic. *Prog. Oceanogr.* **129,** 200–218 (2014).
7. Hawkings, J. R. *et al*. The effect of warming climate on nutrient and solute export from the Greenland ice sheet. *Geochem. Perspect. Lett.* **1,** 94–104 (2015).
8. Hallet, B., Hunter, L. & Bogen, J. Rates of erosion and sediment evacuation by glaciers: a review of field data and their implications. *Glob. Planet. Change* **12,** 213–235 (1996).
9. Koppes, M. N. & Montgomery, D. The relative efficacy of fluvial and glacial erosion over modern to orogenic timescales. *Nat. Geosci.* **2,** 644–647 (2009).
10. Smith, R. W., Bianchi, T. S., Allison, M., Savage, C. & Galy, V. High rates of organic carbon burial in fjord sediments globally. *Nat. Geosci.* **8,** 450–453 (2015).
11. Shepherd, A. *et al*. Reconciled estimate of ice-sheet mass balance. *Science* **338,** 1183–1189 (2015).
12. Enderlin, E. *et al*. An improved mass balance for the Greenland ice sheet. *Geophys. Res. Lett.* **3,** 866–872 (2014).
13. Khan, S. *et al*. Sustained mass loss of the northeast Greenland ice sheet triggered by regional warming. *Nat. Clim. Change* **4,** 292–299 (2015).
14. Howat, I., Joughin, I. & Scambos, T. A. Rapid changes in ice discharge from Greenland outlet glaciers. *Science* **315,** 1559–1561 (2007).
15. Moon, T., Joughin, I., Smith, B. & Howat, I. 21st century evolution of Greenland outlet velocities. *Science* **336,** 576–578 (2012).
16. van der Broeke, M. *et al*. On the recent contribution of the Greenland ice sheet to sea level change. *Cryosphere* **10,** 1933–1946 (2016).
17. Hudson, B. *et al*. MODIS observed increase in duration and spatial extent of sediment plumes in Greenland fjords. *Cryosphere* **8,** 1161–1176 (2014).
18. Hasholt, B. *et al*. Sediment transport to the Arctic Ocean and adjoining cold oceans. *Nord. Hydrol.* **37,** 413–432 (2006).
19. Ettema, J. *et al*. Climate of the Greenland ice sheet using a high-resolution climate model—Part 1: evaluation. *Cryosphere* **4,** 511–527 (2010).
20. Noël, B. *et al*. Evaluation of the updated regional climate model RACMO2.3: summer snowfall impact on the Greenland ice sheet. *Cryosphere* **9,** 1831–1844 (2015).
21. Morlighem, M., Rignot, E. & Mouginot, J. Deeply incised submarine glacial valleys beneath the Greenland ice sheet. *Nat. Geosci.* **7,** 18–22 (2014).
22. Howat, I., Negrete, A. & Smith, B. The Greenland Ice Mapping Project (GIMP) land classification and surface elevation datasets. *Cryosphere* **8,** 1509–1518 (2014).
23. Joughin, I., Smith, B., Howat, I. M., Scambos, T. & Moon, T. Greenland flow variability from ice-sheet-wide velocity mapping. *J. Glaciol.* **56,** 415–430 (2010).
24. Escher, J. C. & Pulvertaft, T. C. R. *Geological map of Greenland* 1: 2500000 (Geological Survey of Denmark, 1995).
25. Arrigo, K. R. *et al*. Melting glaciers stimulate large summer phytoplankton blooms in southwest Greenland waters. *Geophys. Res. Lett.* **44,** 6278–6285 (2017).
26. Meire, L. *et al*. Glacial meltwater and primary production are drivers of strong CO2 uptake in fjord and coastal waters adjacent to the Greenland ice sheet. *Biogeosciences* **12,** 2347–2363 (2015).
27. Petrenko, D., Podznyakov, D. J., Johannessen, J., Counillion, F. & Sychov, V. Satellite-derived multi-year trend in primary production in the Arctic Ocean. *Int. J. Remote Sens.* **34,** 3903–3937 (2013).
28. Sepulveda, J., Pantoja, S. & Hughen, K. A. Sources and distribution of organic matter in northern Patagonia fjords, Chile (44–46° S): a multi-tracer approach for carbon cycling. *Cont. Shelf. Res.* **31,** 315–329 (2011).
29. Dürr, H. H. *et al*. Worldwide typology of nearshore coastal systems: defining the estuarine filter of river inputs to the oceans. *Estuar. Coast.* **34,** 441–458 (2011).
30. Mankoff, K. D. *et al*. Structure and dynamics of a subglacial discharge plume in a Greenlandic fjord. *J. Geophys. Res.* **121,** 8670–8688 (2016).

Acknowledgements

I.O. and B.H. were supported by NSF-OPP award ARC-0909349. M.R.v.d.B. and B.P.Y.N. received funding from NWO/NPP and the Netherlands Earth System Science Centre (NESSC). We thank I. Joughin and E. Enderlin for data sharing. S. Frye, NASA-GSFC, enabled acquisition of ALI imagery.

Author contributions

I.O. and B.H. designed the study and implemented the analysis. J.P.M.S., B.H., A.B.M. M.R.v.d.B., M.M. and B.P.Y.N. contributed to data analysis. I.O. authored the manuscript, all co-authors contributed to the writing.

Additional information

Supplementary information is available in the online version of the paper. Reprints and permissions information is available online at www.nature.com/reprints. Publisher's note: Springer Nature remains neutral with regard to jurisdictional claims in published maps and institutional affiliations. Correspondence and requests for materials should be addressed to I.O.

Competing financial interests

The authors declare no competing financial interests.

Methods

Suspended sediment concentration sampling. We use three field sites in Greenland (Supplementary Fig. 1) to obtain *in situ* suspended sediment concentration (SSC) measurement to relate to visible and near-infrared light reflectance as measured with the Landsat7 satellite. The Watson River has the most comprehensive monitoring data set of any river in Greenland. Typically, its river channel is frozen from October through May, with peak flows during the summer season[31]. We combine all available *in situ* SSC measurements and then correlate these measurements to collocated Landsat reflectance data (Supplementary Table 1). Three locations along this river system have been used.

Location (1). The Watson River originates near the Greenland ice sheet margin from the Russell Glacier and the Leverett Glacier (at 67°04′ N, 50°13′ W, Supplementary Fig. 1). Near the snout of the Leverett Glacier, 49 suspended sediment concentration measurements were collected by Bartholomew and colleagues[32]. We compared seven *in situ* samples collected on the same day to reach-averaged Landsat7 Band 4 values. These measurements were collected in the summer of 2009 and included the highest SSC value in the study, 7,060 mg l^{-1} on 7 August 2009.

Location (2). At the town of Kangerlussuaq, a river gauging station has been maintained continuously since 2007 (at 67°00′ N, 50°41′ W)[31]. Sediment concentration samples included 1l and 0.5l bottle and automated suction pump samples, which were collected daily during the melt seasons of 2007–2014. A total of 27 SSC–Landsat same-day matchups between 2007 and 2012 are established from the available samples.

Location (3). In Kangerlussuaq Fjord on 23 July 2012, 15 SSC samples were collected from the river mouth near-coincident with an acquisition of NASA Advanced Land Imager (ALI). All surface water samples on this day were collected between 15 min before and 2 h and 37 min after the ALI image was acquired.

Combined, these samples provide a complete coverage of the active river discharge season subsequently analysed (day 140–day 240).

Landsat 7 ETM+ and EO-1 ALI imagery. Landsat 7 Enhanced Thematic Mapper Plus provides global imagery at 30 m resolution in relevant reflective bands and repeats every 16 days. Landsat images were downloaded for all days that SSC samples existed from the USGS Earth Explorer archive[33].

A shortwave infrared band (Landsat7 Band 5, wavelength 1,550–1,750 nm) was used to differentiate water from land, utilizing water's strong absorption of light in the near-infrared wavelengths. A threshold of Band 5 reflectance of <0.05 was used to classify water. To quantify SSC in the river water we use Band 4 reflectance (wavelength 770–900 nm).

We acquired an on-demand image of the Earth Observer-1 ALI to calibrate SSC samples collected on 23 July 2012. Spatial resolution of ALI is 30 m, the same as Landsat7 images. ALI has two near-infrared bands (MS- 4 775–805 nm and MS- 4′ 845–890 nm). To make these measurements comparable to Landsat7 Band 4, the reflectance from these two bands were averaged for our analysis. All images were processed from calibrated digital number to reflectance following protocols by Chander and colleagues[34]. All calibration images were manually checked for cloud contamination.

SSC retrieval algorithm. The combined data set of satellite imagery and observed suspended sediment concentration was used to develop a SSC retrieval algorithm:

$$\mathrm{SSC} = 4.74\, e^{38.35 * \mathrm{RB4}} \quad (R^2 = 0.90, n = 49) \tag{3}$$

where R_{B4} is the reflectance value from Landsat 7, Band 4, and the average ALI $R_{MS\text{-}4}$ reflectance (-), and SSC is suspended sediment concentration in mg l^{-1}. Supplementary Fig. 2 shows the supporting data and best fit, and Supplementary Table 1 lists all data points and the Landsat7 and ALI near-infrared reflectance. The mean standard error of the estimate of this relationship is ±625 mg l^{-1}.

SSC retrieval algorithm application to Landsat7. The established reflectance-SSC retrieval algorithm was applied to the entire Landsat7 data catalogue (1999–2013) through Google Earth Engine. We restricted our analysis to snow-free periods and the active river discharge season between year day 160 through 240.

We created a map of median SSC for all appropriate river outlets around the entire ice sheet margin from all Landsat7 images. Suspended sediment concentration measurements typically include a large range of values, which led us to use the median SSC over all water pixels across transects in the braidplain. Close proximity of selected transects to the ice margin (<2 km) guarantees there is limited resuspension of sediment within the floodplain.

The following processing steps were implemented:

(1) Images with >50% cloud cover were removed, utilizing the Landsat7 internal cloud cover metadata field.
(2) Poorly geo-located images were removed when Google Earth Engine's internal image registration statistics deviated more than 100 m (3 pixels) from the reference image.
(3) Imagery was processed to top of the atmosphere reflectance according to ref. 34.
(4) Our script classified a pixel as water if Landsat 7 Band 5 reflectance was <0.05.
(5) Terrain and cloud shadow effects were minimized, after manual quality control, by only allowing Band 1 reflectance values >0.15.
(6) Thresholds for snow and ice occurrence were established from image inspection and optimization of thresholds for different wavelengths as applied to >100 calibration images. Pixels were classified as snow/ice (and removed) if:
    a. Band 2 reflectance was >0.3
    b. or Band 4 reflectance was >0.25
    c. or Band 5 was >0.28
(7) The persistence of water was measured. Water must have been detected at least ten times before a pixel was classified as river and included in the final analysis.
(8) The retrieval algorithm found in equation (3) was applied to each image to determine SSC.

Only a selected number of rivers have high-quality data on ice thickness in their upstream drainage basin[21]. For these rivers, we extracted time series of SSC by applying two additional steps:

(9) For each region of interest a mean SSC value was calculated for pixels classified as water. The total number and percentage of pixels classified as water was also recorded. For several catchments, we imaged multiple meltwater outlets using multiple regions of interest due to the large size of these termini.
(10) Landsat7 era summary statistics were calculated for each region of interest. For outlets with multiple regions of interest, summary statistics were weighted by the number of images contributing.

All images of locations that exceeded a mean SSC of 3,000 mg l^{-1} were manually checked for clouds.

Delineation of hydrologic catchments. We define contributing on-ice catchments to each outlet based on calculations of the local hydrostatic pressure field[35,36]. To calculate the hydraulic potentiometric surface, φ, we use the aforementioned basal topography and ice surface topography data[21].

$$\varphi = \rho_{\mathrm{ice}} g (z_{\mathrm{ice}} + 0.1 z_{\mathrm{bed}}) \tag{4}$$

where z_{ice} is ice surface topography (m), z_{bed} is basal topography (m), ρ_{ice} is density of ice (900 kg m^{-3}), and g is gravitational acceleration (9.81 m s^{-2}).

Our method takes into account how water pressure equals ice overburden pressure, but it is limited by the resolution of the basal topography, thus the hydraulic potentiometric surface carries significant uncertainty. A D8 flow routing approach[37] implemented in RiverTools determines hydrological catchment characteristics. This specific algorithm is unique in distributing flow proportionally in flat areas, and relies less on pit-filling of the initial elevation maps and may alleviate just concerns on the uncertainty of catchment delineation results[38]. Whereas for small individual on-ice catchments area uncertainty can still be significant, this workflow is considered suited for broad-scale hydrological assessment[35].

RACMO2.3 runoff. The regional-atmospheric climate model, RACMO2.3 combines a high-resolution weather prediction model and the European Centre for Medium-range Weather Forecasts with advanced snow models to determine daily ice sheet surface mass balance[19,27,39,40].

Specifically, we use RACMO2.3 daily runoff output from 1 January 1999 to 31 December 2013. Runoff, R in metres, is defined as the sum of rain and melt, minus local refreeze and retention. Runoff is calculated for the entire Greenland ice sheet at ~11 km resolution. Modelled runoff was validated against a set of measurements in West Greenland in the Watson River drainage area[39] and carries an estimated uncertainty in ice sheet runoff of 20% (ref. 41).

We overlay the delineated catchments with the gridded RACMO2.3 data and sum runoff for all grid cells over a melt year, and multiply by respective grid cell surface area. Mean annual meltwater outflow was then determined over 1999–2013.

$$Q_{\mathrm{mc}} = \frac{1}{m} \sum_{m=1}^{m} \sum_{j=1}^{j} \sum_{i=1}^{i} R_{ijm} A_i \tag{5}$$

where Q_{mc} is meltwater catchment outflow (m^3 yr^{-1}), R is meltwater runoff (m), A is gridcell area (m^2), i is grid index, n is days in summer melt season (that is, days of $R > 0$ m), and m is number of years ($m = 14$).

This summation ignores transmission losses due to refreezing and retention along the glacio-hydrological transport pathway. Infiltration and refreezing may

retain a significant volume of melt water produced at upper elevations of the ice sheet, and thus prevent it from reaching the ice margin and coast[42,43]. Recent work provided new observations of the complexity of the storage of melt water in firn. Recent SMB models show that currently ~40% of the melt water is retained *in situ* at the scale of the model grids. However, aspects of this process remain uncertain[44] and subsequent routing through the glacio-hydrological system may cause additional unaccounted storage[45]. Note that numerically modelled meltwater runoff is higher for downscaled high-resolution implementations[40] due to changes in precipitation patterns, with most profound impacts on the small icecaps.

We assume that critical processes are restricted to those areas of the larger on-ice catchments that generate runoff. We define the active melt catchment, A_{mc} (in m^2) by using only those regions of the delineated hydrological catchment where runoff occurred as predicted by the numerical model.

Calculation of glacier erosion potential. Theory on glacial erosion dictates that abrasion relates to basal sliding[46,47]. To test whether glacial abrasion explains riverine suspended sediment concentration we formulate the first-order erosion potential, EP, as:

$$\mathrm{EP} = u_s \tau = u_s \rho_{ice} g h_{ice} S \quad (6)$$

where u_s sliding ice velocity ($m\,yr^{-1}$), ρ_{ice} is density of ice ($900\,kg\,m^{-3}$), g is gravitational acceleration ($9.81\,m\,s^{-2}$), h_{ice} is ice thickness (m), and S local surface slope provided that slopes are small[36]. We assume $u_s = a\,u_{surf}$ (with $a = 0.8$) to arrive at the bed sliding ice velocity, u_s, from the observed surface velocity, u_{surf} (ref. 36).

The mean erosion potential within the melt catchment, EP_{mc}, is then calculated as:

$$\overline{\mathrm{EP}_{mc}} = \frac{1}{i}\sum_{i=1}^{i}(0.8 u_{surfi} h_i \rho_{ice} g S_i) \quad (7)$$

where u_{surf} mean annual surface ice velocity ($m\,yr^{-1}$) and i is the grid index.

Ice thickness is derived from the basal topography[21], in combination with the surface topography[22].

Ice surface velocity is derived from analysis of repeat RADAR-SAT1 measurements for the 2005–2006 winter[23]. The 2005–2006 data set is selected as it measured ice surface velocities in the middle of the Landsat7 record. Surface velocity data (at 500 m resolution) was linearly interpolated to match the resolution of ice thickness data (at 150 m resolution).

Classification of rock strength. We use the Greenland map of geology[24], which covers the exposed bedrock of coastal Greenland. Greenland comprises for the largest part of crystalline rocks of the Precambrian Shield of Greenland, mainly orthogneisses. Younger sedimentary basins formed during the Proterozoic eon and throughout the Phanerozoic eon, most notably in Northern and East Greenland (limestones and dolomites, amongst others).

The lithological descriptions from the geologic map define a rock strength classification based on the Schmidt Hammer scale: 40–50 for moderately strong rock, as is observed in competent sedimentary rock, 50–60 for strong rock, as in igneous and metamorphic rock, and up to 65 for dense fine-grained igneous and metamorphic rocks (basalt, amongst others)[48].

Calculation of sediment load. We estimate the mean annual total suspended sediment load, Qs in $kg\,yr^{-1}$, for 160 ice sheet termini individually:

$$\overline{Qs} = \frac{1}{m}\sum_{j=1}^{m}\sum_{i=1}^{n} Q_{mc}\mathrm{SSC} \quad (8)$$

Long-term SSC values were assumed a representative concentration for all water discharges. Greenlandic rivers are turbulent and shallow, and thus suspended sediment concentrations are assumed to be relatively well-mixed. Although these river systems most probably still have a modest increase of sediment concentration with depth, because we lack information to constrain vertical concentration profiles we have made no attempt to extrapolate a possible increase in SSC with depth.

We calculated total sediment export (Qs_{total}) from the Greenland ice sheet by melt water with two different methods: Direct upscaling of the SSC to entire GrIS meltwater flux; and extrapolation of the established SSC to ice dynamics relationship to all GrIS glaciated basins.

Meltwater flux ratio method. Assuming our data set of 160 rivers around the Greenland ice sheet margin captures the variability of all on-ice catchments producing meltwater discharge, we upscale the measured sediment concentration and water flux directly to the total freshwater discharge produced. Our data set samples ~17% of the total meltwater flux of Greenland.

$$Qs_{GrIS} = Qs_{measured}\frac{Q_{GrIS}}{Q_{measured}} \quad (9)$$

where Qs_{GrIS} is total sediment load for Greenland ice sheet ($kg\,yr^{-1}$), $Qs_{measured}$ is total sediment load for all satellite-measured river outlets ($kg\,yr^{-1}$), Q_{GrIS} is total outflow for Greenland ice sheet from RACMO2.3 ($m^3\,yr^{-1}$), and $Q_{measured}$ is total outflow for all satellite-measured river outlets ($m^3\,yr^{-1}$)

For an average of ~71 km^3 of water, which RACMO2.3 models to be leaving the ice sheet per year for the included on-ice catchments, we estimate with Landsat7 measurements $0.216\,Gt\,yr^{-1}$ of sediment is exported. RACMO2.3 1999–2013 yearly mean runoff and reconciled estimates calculate a total freshwater flux of 418 km^3 of water discharged from the entire GrIS annually, which implies approximately $1.28\,Gt\,yr^{-1}$ would be exported with this freshwater discharge.

The uncertainty in this estimate, η_{Qs}, can be quantified from the summation of the error in the reconstructed SSC over the mean SSC of all 160 river outlets, and the estimated error in the reconstructed discharge from the RACMO model (20%):

$$\eta_{Qs} = \sqrt{\left(\frac{625}{\mathrm{SSC}_{mean}}\right)^2 + 0.2^2} \quad (10)$$

Thus, the relative error amounts to 40%, and our reconstructed total sediment load amounts to $1.28 \pm 0.51\,Gt\,yr^{1}$.

Extrapolation of SSC–ice dynamics relationship. We find SSC is controlled by ice dynamics, particularly basal shear and ice surface velocity. The mean standard error of the estimate of this relationship is $\pm 471\,mg\,l^{-1}$. This relationship allows for a physically based method to estimate sediment export for all catchments of the GrIS. We map surface velocity, ice thickness, and runoff for all glacio-hydrological catchments along the entire ice sheet. We then calculate for each catchment the relevant values needed to calculate median catchment SSC with equation (7). Finally, we utilize calculated catchment-specific median SSC with the mean yearly runoff from RACMO2.3, to arrive at a sediment load estimate for each catchment. The sediment load reconstruction for entire Greenland is then the summation of all delineated catchments, and amounts to $0.892\,Gt\,yr^{-1}$.

Similarly, uncertainty in the estimate can be quantified from the summation of the error in the reconstructed SSC from the glacier dynamics relationship over the mean SSC of 58 selected outlets, $SSC_{glacdyn}$, and the estimated error in the reconstructed discharge from the RACMO model (20%):

$$\eta_{QsEP} = \sqrt{\left(\frac{471}{\mathrm{SSC}_{glacdyn}}\right)^2 + 0.2^2} \quad (11)$$

In this case, the relative error amounts to 42%, and our reconstructed total sediment load amounts to $0.892 \pm 0.374\,Gt\,yr^{-1}$.

This method does justice to the variability of suspended sediment load due to differences in glacier flow dynamics, and at the same time uses the meltwater flux per basin as the transporting mechanism for the eroded sediment. However, the method extrapolates past the range of the observed data used to determine equation (6). Since this extrapolation is most profound at the fast-moving tidewater glacier outlets, we choose to limit our extrapolation to the uppermost limit of the observed samples ($7{,}000\,mg\,l^{-1}$). True calibration data for these locations cannot be accomplished with the described technique, but future data collection on SSC near tidewater outlets would reduce uncertainty in the reconstructed total sediment load for Greenland.

Additional flux of sediment transported by calving ice. Our methodology does not allow direct measurement of either the englacial and basal ice flux of sediment in icebergs, or for suspended sediment transported in the supraglacial transport system. We assume that suspended sediment concentration in the supraglacial system is negligible, with exception of only a few outlets, and we exclude this component from our analysis. However, to put the sediment budget of all meltwater transport into perspective into the overall sediment transport for the entire GrIS, we here estimate sediment originating from calving fronts along the Greenland ice sheet margin.

We use a reconstructed average GrIS calving ice discharge, $Q_{calving}$, of $\sim 519 \pm 10\,Gt\,yr^{-1}$ over 2000–2012[12]. This calving ice discharge estimate is based on a compilation of radar thickness data and velocity reconstructions for 178 individual calving fronts with termini wider than 1 km. This study used an ice density, ρ_{ice}, of $900\,kg\,m^{-3}$ to convert ice volume to ice mass flux (consistent with ref. 12), and a sediment density, ρ_{sed}, of $2{,}500\,kg\,m^{-3}$ to convert sediment volume to sediment mass.

Englacial sediment, debris and dust held throughout the ice column, will be released over the entire period of melt of calved icebergs (Supplementary Fig. 3). This component of ice-transported sediment thus has higher travel distances. In terms of sediment budget, this component is most similar to suspended sediment delivered by proglacial river discharge.

We use an englacial sediment concentration of ~0.001%, based on rare field observations of englacial sediments at a calving front in Baffin Island[48]. Assuming a

uniform englacial sediment concentration throughout the entire ice volume, the annual total flux of englacial sediment (in kg yr^{-1}) is calculated as follows:

$$Qs_{\text{englacial}} = 0.00001 \frac{Q_{\text{calving}}}{\rho_{\text{ice}}} \rho_{\text{sed}} \quad (12)$$

where $Qs_{\text{englacial}}$ is total annual sediment load from englacially transported sediment (kg yr^{-1}) and Q_{calving} is total annual calving glacier water flux (m^3 yr^{-1})

Thus, calving ice results in ~0.014 Gt of fine englacial sediment release into fjords and the coastal ocean each year.

Additionally, the calving ice front contains a debris-rich basal layer (Supplementary Fig. 3). Field observations of this layer in icebergs range between 1 and 4 metres in thickness, we here use an average of thickness of the debris and sediment-rich basal layer, T_{basal}, of 3 m (ref. 49). When we assume an average calving front thickness, T_{cf}, of 300 m; approximately 1% of the calving ice mass consists of debris-laden ice. Andrews *et al.*[50] estimate a sediment concentration of 20% by volume in the basal layer.

$$Qs_{\text{basal}} = 0.002 \frac{Q_{\text{calving}}}{\rho_{\text{ice}}} \rho_{\text{sed}} \frac{T_{\text{cf}}}{T_{\text{basal}}} \quad (13)$$

where Qs_{basal} is total annual sediment load from basal sediment (kg yr^{-1}) and Q_{calving} is total annual calving glacier water flux (m^3 yr^{-1})

The estimated basal sediment flux then amounts to ~2.88 Gt yr^{-1}.

Code availability. The data processing scripts are available in GitHub (https://github.com/BDHudson/Greenland-SedimentFlux/blob/master/Code/CalcSedFlux_October2016.ipynb). The RACMO2.3 surface mass balance code is open source and available from MvDB, Utrecht University, but the coupled atmosphere–ocean model is not in the open-source domain.

Data availability. The data supporting the findings of this study are available within the article and its supplementary information files.

References

31. Chu, V. W., Smith, L. C., Rennermalm, A., Forster, R. & Box, J. E. Hydrological controls on coastal suspended sediment plumes around the Greenland ice sheet. *Cryosphere* **6,** 1–19 (2012).
32. Hasholt, B., Mikkelsen, A. B., Nielsen, M. H. & Larsen, M. Observations of runoff and sediment and dissolved loads from the Greenland ice sheet at Kangerlussuaq, West Greenland, 2007 to 2010. *Z. Geomorphol.* **57 (suppl.),** 3–27 (2013).
33. Bartholomew, I. *et al*. Supraglacial forcing of subglacial drainage in the ablation zone of the Greenland ice sheet. *Geophys. Res. Lett.* **38,** 1–5 (2011).
34. Woodcock, C. E. *et al*. Free access to Landsat imagery. *Science* **320,** 1011 (2008).
35. Chander, G., Markham, B. L. & Helder, D. Summary of current radiometric calibration coefficients for Landsat MSS, TM, ETM+, and EO-1 ALI sensors. *Remote Sens. Environ.* **113,** 893–903 (2009).
36. Lewis, S. M. & Smith, L. C. Hydrologic drainage of the Greenland ice sheet. *Hydrol. Process.* **23,** 2004–2011 (2009).
37. Cuffey, K. M. & Paterson, W. S. B. *The Physics of Glaciers* 4th edn, 693 (Elsevier, 2010).
38. Tarboton, D. A new method for the determination of flow directions and contributing areas in grid digital elevation models. *Wat. Resour. Res.* **33,** 309–319 (1997).
39. Yang, K., Smith, L. C., Chu, V., Gleason, C. & Li, M. A caution on the use of surface digital elevation models to simulate supraglacial hydrology of the Greenland ice sheet. *IEEE J-STARS* **8,** 5212–5224 (2015).
40. Ettema, J., van den Broeke, M. R., van Meijgaard, E. & van den Berg, W. J. Climate of the Greenland ice sheet using a high-resolution climate model—Part 2: near-surface climate and energy balance. *Cryosphere* **4,** 529–544 (2010).
41. Noël, B. *et al*. Summer snowfall on the Greenland ice sheet: a study with the updated regional climate model RACMO2.3. *Cryosphere* **9,** 1177–1208 (2015).
42. Bamber, J., van den Broeke, J. M. R., Ettema, J., Lenaerts, J. & Rignot, E. Recent large increases in freshwater fluxes from Greenland into the North Atlantic. *Geophys. Res. Lett.* **39,** L19501 (2012).
43. Harper, J., Humphrey, N., Pfeffer, W. T., Brown, J. & Fettweis, X. Greenland ice-sheet contribution to sea-level rise buffered by meltwater storage in firn. *Nature* **491,** 240–243 (2012).
44. Janssens, I. & Huybrechts, P. The treatment of meltwater retention in massbalance parameterizations of the Greenland ice sheet. *Ann. Glaciol.* **31,** 133–140 (2000).
45. van Angelen, J., Lenaerts, J., van den Broeke, M. R., Fettweiss, X. & van Meijgaard, E. Rapid loss of firn pore space accelerates 21st century Greenland mass loss. *Geophys. Res. Lett.* **40,** 2109–2113 (2013).
46. Overeem, I. *et al*. River inundation suggests ice sheet runoff variations. *J. Glaciol.* **61,** 776–788 (2015).
47. Hallet, B. A theoretical model of glacial abrasion. *J. Glaciol.* **23,** 39–50 (1979).
48. Goudie, A. S. The Schmidt hammer in Geomorphological research. *Prog. Phys. Geogr.* **30,** 703–718 (2006).
49. Dowdeswell, J. A. & Murray, T. in *Glacimarine Environments: Processes and Sediments* Vol. 53 (eds Dowdeswell, J. A. & Scourse, J. D.) 1121–1137 (Geological Society Special Publication, 1990).
50. Andrews, J. T., Milliman, J. D., Jennings, A. E., Rynes, N. & Dwyer, J. Sediment thicknesses and holocene glacial marine sedimentation rates in three East Greenland Fjords (ca. 68° N). *J. Geol.* **102,** 669–683 (1994).